Applied Surface Science 492 (2019): 362-368

DOI: https://doi.org/10.1016/j.apsusc.2019.06.056

Near ambient pressure X-ray photoelectron spectroscopy monitoring of the surface immobilization cascade on a porous silicon-gold nanoparticle FET biosensor

Chloé Rodriguez[1,2], Paul Dietrich[3], Vicente Torres-Costa[1,4], Virginia Cebrián[2], Cristina Gómez-Abad[2], Ana Díaz[2], Oscar Ahumada[2], Miguel Manso Silván[1]*

[1]Departamento de Física Aplicada and Instituto de Ciencia de Materiales Nicolás Cabrera, Universidad Autónoma de Madrid, 28049, Madrid, Spain

[2]Mecwins S.L., Parque Científico de Madrid PTM, C/Santiago Grisolía 2, Tres Cantos, 28760, Madrid, Spain

[3]SPECS Surface Nano Analysis GmbH. Voltastrasse 5, 13355 Berlin, Germany

[4]Centro de Microanálisis de Materiales, Universidad Autónoma de Madrid, 28049, Madrid, Spain

*corresponding author: miguel·manso@uam·es, tel: +34 914974918

Abstract

Porous silicon (PSi) offers extremely attractive optical, electronic and biofunctional properties for the development of biosensors. In the present work, we have studied the step by step sandwich biofunctionalization cascade of a PSi platform by near ambient pressure X-ray photoelectron spectroscopy (NAP-XPS) and, in parallel, we have developed a three electrode PSi device sensitive to changes in surface conductance. Prior to the NAP-XPS characterization, the organosilanization with glycidyloxy-propyl-trimethoxy-silane, the bioconjugation, and the gold nanoparticle (AuNP) sensitization layer were monitored by spectroscopic ellipsometry. The NAP-XPS analysis revealed outstanding results: a) the NAP-XPS chamber allows detecting the pristine PSi with negligible adventitious carbon contamination, b) the single oxygen bonded carbon component of the Glycidyl group dominates the C1s core level after organosilanization, c) the good progress of the biofunctionalization/recognition is confirmed by the increase of the silica to silicon component ratio in the Si2p core level and, d) the N1s core level describes identical features from the presence of aminoacid sequences in the capture/detection steps. A FET sensing of a prostate specific antigen (PSA) marker was performed through conjugation with AuNPs. For a given concentration of PSA (and AuNPs) the conductance increased with the increase of the gate voltage. For a given gate voltage, the conductance was observed to increase for increasing concentration of PSA. This allowed proposing a calibration line for the biosensor, which is valid from a clinically relevant range of 0.1 ng/mL.

Keywords: porous silicon, biosensor, near ambient pressure X-ray photoelectron spectroscopy, FET, sandwich bioassay, gold nanoparticles.

1 Introduction

Biosensing devices are to play a fundamental role in an increasingly concerned world with growing demands of environmental, security and health monitoring. Biosensors are composed of three main parts: a transductor (responsible of altering a physical signal), a biointerface (that should ensure that signal activation is only induced upon specific recognition, most often immunological or DNA hybridization reactions) and a target biomolecule (also known as marker, that identifies as univocally as possible the its presence with the biological process in question) [1]. The optimization of a biosensor can take place through modifications of any of these aspects, but the biointerface is critical since it interconnects the whole system once the transductor and the target biomolecule are given [2].

The biointerface preparation requires a series of steps, which constitute the biofunctionalization cascade. The first stage is devoted to create a transition from the generally inorganic transductor to the organic nature of the biomolecules. Secondly, a crosslinker/spacer that shall bind a trapping biomolecule with no interference of its biomolecular activity is used. Finally, the trapping molecule itself (of immunologic [3], nucleic [4] or aptameric nature [5]) is immobilized on top. In particular cases, intermediate binding proteins (which have no intrinsic detection role), such as protein A, can be used to optimize the orientation/activity of the trapping molecule [6]. This protein is isolated from Staphylococcus aureus cell wall and allows increasing, in a species dependent manner, the binding constant of immunoglobulins to porous surfaces [7]. The biofunctionalization cascade should lead to surfaces with high densities of surface available and active trapping molecules.

Surface characterization techniques are to play a fundamental role in the optimization of biofunctionalization cascades. Two classes of techniques can be

complementary used to monitoring the development of the biointerface: dynamic techniques and spectroscopic techniques. The former allow a kinetic monitoring of the process of molecular binding on the surface by changes in mass (i.e. quartz crystal microbalance [4]) or refractive index (i.e. through ellipsometry [8] or surface plasmon resonance [9]). The second family of techniques provides atomic or molecular evidence of presence of relevant species required in the control of the biosensor interface. Vibrational (especially attenuated total reflection Fourier transformed infrared spectroscopy [10]), photoelectron (X-ray photoelectron spectroscopy, XPS [6]) and mass spectroscopies (time of flight secondary ion mass spectroscopy, ToF-SIMS [11]) outstand in this role of controlling the surface properties at each stage of development of the biofunctionalization cascade.

New technological developments have allowed proposing novel vacuum spectroscopic equipment to work in nearly environmental conditions. ToF-SIMS has for instance been used to characterize water clusters while running water through a microfluidic device [12]. In parallel, near ambient pressure XPS (NAP-XPS, referred also in bibliography to Atmospheric Pressure Photoelectron Spectroscopy, APPES) has been used to characterize a diversity of solid-liquid interfaces [13]. Recently, the use of NAP-XPS has broken the barriers of reaching biointerfaces problems [14].

In this work we aim at describing the process of biofunctionalization of a porous silicon sensing interface by using ellipsometry and NAP-XPS. The biofunctionalization cascade consists of a glycidyloxy-propyl-trimethoxy-silane (GPMS) layer [15] and an immobilized prostate specific antigen (PSA) antibody, which is completed upon recognition in a sandwich assay with a PSA detection antibody conjugated gold nanoparticles (AuNPs). These nanoparticles play a role in the electrical sensitization of the surface [16], which has allowed us to propose a detection of the PSA marker by

implementing a three electrode field effect transistor (FET) prototype biosensor, working similarly as proposed for other nanostructured [5] and porous [17] silicon devices.

2. Experimental

The step by step process of preparation of the PSi-AuNPs FET device and the critical steps of the biofunctionalization cascade are presented schematically in figure 1.

2.1 Fabrication of the PSi FET.

Si wafers ([100] orientation, p-type, B doped, resistivity 0.05–0.1 Ω.cm) were first coated with an Al film (e-beam evaporation) on the non-polished side. After rapid thermal annealing a low resistance ohmic electrical contact was formed. The wafer was then cut into 15 × 15 mm^2 squares. For the formation of PSi, the samples were mounted into a Teflon cell working as electrochemical anode. Sponge-like PSi was grown by etching the silicon wafer in hydrofluoric acid (HF) and absolute ethanol at a volume ratio of 1:1. For the given Si substrate and electrolyte properties, the porosity of the anodized films is determined by the current density during anodization (and illumination conditions, not considered in this work). A mesoporous columnar Si layer was grown following previous conditions [6] with a current density fixed at 80 mA/cm^2, and an anodization time of 20 s, giving rise to a 1 μm thick film. Finally, the formed PSi was rinsed with ethanol and dried under N_2 flow.

Two additional Ni/Cr electrical contacts were grown on the PSi surface [18]. The contacts were deposited 250 nm deep into PSi by carving two slots using Ar^+ ion etching (0.5 keV, up to 0.6 C total charge) through a Si mask as previously done in interdigitated systems [16]. Ni/Cr (40/60 wt %) contacts were then sputtered through the

mask during 5 min in an Ar^+ discharge (fed at 0.5 kV, 1 A) at a working pressure of 10^{-2} mbar. After Si mask removal, the PSi based device consisted of an Al back gate contact and two surface NiCr contacts.

The electrical characterization of all the PSi-FET structures was performed by measuring I-V characteristics (SP-150 instrument, Bio-Logic Science Instruments) between the PSi surface electrodes while feeding the back Al contact with a specific gate voltage (Keithley 2400 SourceMeter) in the 0-2V range with 0.5 V steps.

2.2 PSi biointerface.

In order to initiate the organo-silanization of the surface, PSi was first oxidized in H_2O_2/EtOH solution at 1:1 volume ratio. This reaction is key in the mechanical stabilization the PSi stratum and in the efficiency of the ulterior epoxy-silanization, which took place at room temperature with GPMS (Sigma-Aldrich) in methanol at 1:1000 volume ratio. A spontaneous condensation reaction between the SiOH groups formed by the chemical oxidation of the PSi surface and the organosilane follows [6].

The sandwich assay was initiated by immobilization of the capture antibody (monoclonal mouse anti-PSA 1H12 antibody, 50 μg/mL, HyTest, Turku, Finland) on GPMS-PSi interface for 2 h at 37ºC, in 10 mM 2-morpholinoethanesulfonic acid (MES) at a pH of 3.8. In order to avoid non-specific interactions, the surface was then blocked overnight at 4ºC with (aminoethyl)polyethylene glycol (PEG) (Sigma-Aldrich) at 1 mg/mL in 10 mM MES and 0.05% Tween® (pH 5.5). Then, the immunoreaction between the marker (PSA) and the 1H12/GPMS/PSi interfaces takes place in fetal bovine serum (FBS) 1x in a range of PSA concentrations from 0.1 to 100 ng/mL (HyTest, Turku, Finland) at 37ºC. A control 1H12/GPMS/PSi sample is performed in FBS with no addition of PSA.

The sandwich assay is completed by immersion for 1h at 37ºC of the PSA/1H12/GPMS/PSi samples in a 5 μg/mL solution of AuNPs. Chosen AuNPs were spherical, of 100 nm diameter and coated with 2-3 nm long thiol-spacer-carboxyl (C11-100-TC-50, NanopartzTM). These were previously conjugated with a PSA detection antibody (anti-PSA 5A6 antibody, HyTest, Turku, Finland) prepared in MES (pH 3.8) with 0.05% Tween® [19]. The PSi biointerfaces were prepared in 4 replicates at each PSA concentration, three of them with electrical contacts for determination of the FET characteristics after recognition with the detection antibody conjugated with the AuNPs, and a fourth model sample with no electrodes for surface characterization.

2.3 Surface characterization

Ellipsometry measurements were performed in a J.A. Woollam Co. VASE ellipsometer. Data were acquired in the 250−1450 nm range at 70º incidence angle. The results were fitted to an increasingly complex structure according to the biofunctionalization stage. The PSi layer was fitted using a three material effective medium approximation (EMA) model consisting of Silicon, silicon dioxide and air. The composition of this layer was a fitting parameter of the process. A diffusing interface between the Si substrate and the PSi layer was also considered in the model and fitted. A discontinuous surface organic layer was also simulated with an EMA layer considering polymethylmethacrylate as the organic phase and air as the discontinuity. The results are presented as best values of the fitting process with error selected as the maximum value of the standard deviation for that parameter in each of the biofunctionalization steps. The morphology of the NiCr contacts deposited on carved PSi surface were observed by field emission scanning electron microscopy (JEOL JSM 6335F, Centro Nacional de Microscopía Electrónica).

NAP-XPS spectra were obtained in an EnviroESCA Spectrometer (SPECS GmbH). EnviroESCA enables analyses under environmental conditions (near-ambient pressures) far above UHV. It is designed for high-throughput analysis and offers very short loading-to-measurement times on all types of samples opening up new applications in the characterization of wet biomedical and biotechnological samples. The data were processed using CasaXPS v16R1 (Casa Software, UK) taking both the C1s hydrocarbon at 285.00 eV and the Si2p with elemental Si at 99 eV and oxidized Si at 103 eV as binding energy (BE) references and using Gaussian-Lorentzian function (G/L = 30) for core level envelopes and a Shirley baseline. The different components were constrained to present BE widths within 10% differences. The number of components was defined by the presence of maxima and peak asymmetries, in coherence with the existence of references detailing the corresponding chemical assignments. In the case of Au4f peak, an additional area constrain regarding nominal differences between different spin components was considered; the area of the $4f^{7/2}$ component divided by the area of the $4f^{5/2}$ component could not differ in more than 10% from the factor 4/3.

3. Results and discussion

3.1 Characterization of the Biointerface.

The different stages of functionalization of the PSi surface were initially characterized by ellipsometry. The data were fitted through appropriate models to extract relevant parameters for the description of the evolving biointerface. The parameters make reference to the porosity and thickness of the different layers conforming the functionalized PSi biointerface. A scheme of the fitted structure can be observed in the inset of figure 2. Two examples of fitted ellipsometric curves are

presented in supplementary figure S1. By considering first the evolution of the porosity of the PSi structure (Figure 2, left), we were able to confirm that the porosity of PSi decays gradually at each biofunctionalization stage from circa 65% for the pristine PSi to circa 45% upon completion of the biorecognition with conjugated AuNPs. The presence of a Si phase is observed to evolve gradually with a decay in favor of the SiO_2 phase (see right axis in figure 2. Left). It is worth noting that, since the porosity and Si concentration are interrelated with the concentration of SiO_2 ([Si]+[SiO2]+[air]= 100% vol.), it is derived that the biofunctionalization induces an oxidation of the PSi structure (which is partially induced in purpose) and the consequent volume increase of a factor of 2.8 in the Si-Si to Si-O-Si transformation reduces the total porosity. On the other side, the organic layer was observed to become progressively packed/densified upon progress of the biofunctionalization steps; being absent in the PSi control (100% porous organic layer), it becomes relatively dense (10 % porosity) after completion of the detection with the conjugated AuNPs.

The evolution of the thickness of each of the layers considered in the simulation is plotted in the right chart of Figure 2. The thickness of the different PSi layers was observed to slightly vary from one sample to the other, remaining in the 990-1150 nm range, which is related to the PSi fabrication stage rather than to the biofunctionalization (see right axis). On the other hand, the transition layer was observed to slightly decrease (from 50 to 30 nm), in agreement with the transformation of Si into SiO_2, which increases the abruptness of the Si-PSi interface. Relevantly, the thickness of the organic layer monotonically increased from 0 nm up to 90 nm from the pristine PSi to the PSi surface after recognition with a detection antibody conjugated AuNPs. Though this layer may be overestimated in thickness, we shall consider that this value takes into account a second transition layer (from PSi to the organic layer) that was not taken into

account to limit the complexity of the simulations. However, both the previously mentioned discontinuity of this film, and an additional surface roughness parameter (see figure 2 right, left axis) give an additional idea of the complexity of this layer. It is worth mentioning that the evolution of the roughness was coherent with the progress of the biofunctionalization cascade and recognition: a continuous decrease of observed until an increase induced by the presence of the AuNPs.

The surfaces of the PSi were additionally characterized by NAP-XPS (1 mbar Ar pressure) at the different stages of biofunctionalization and sandwich recognition with 100 ng/mL PSA and AuNPs. The Si2p core level spectra shown in figure 3, left, evidence the progressive oxidation of the PSi structure during biofunctionalization and recognition. The spectra were not normalized to qualitatively illustrate the effects of the progressing biofunctionalization. In this case, the surface Si composition is observed to decrease as the surface biofunctionalization progresses. The spectrum of the pristine PSi shows a dominant Si2p component at the binding energy (BE) of 99.0 eV corresponding to Si-Si bonding, which could be used as additional signal for calibration of the BE. Upon organo-silanization, the surface drastically changes, showing a dominant Si-O component at a BE of 103.0 eV, issuing from both, the PSi induced oxidation and the detection of Si-O in bound GPMS, in agreement with what observed upon biofunctionalization of PSi with other organosilanes [6, 20] including variable angle detection [21]. By further progressing in the biofunctionalization (capture antibody immobilization (ab_1)) and detection (recognition of PSA and sandwich with the detection antibody (ab_2) conjugated AuNPS), the Si-Si component of the PSi surface appears attenuated due to the increasing thickness of the bio-organic layer above.

The spectra shown in the middle graph of figure 3 correspond to the C1s core level spectra of the same samples. The progress of the biofunctionalization/detection

stages induced an increase of the overall C content on the surface. Outstandingly, the spectra show that the pristine PSi surface presents almost no adventitious carbon. This result suggests a protective effect of the surface adsorbed water on the PSi surface and on the future potential use of NAP-XPS for performing in situ surface modification of biosensors in water solution to avoid cross reactivity. The surface of the GPMS silanized PSi shows a profile dominated by two main components, with a dominant component at 286.5 eV BE associated to the single bonded C-O-C structure of the glycidyloxy group and a secondary component associated to the aliphatic propyl chain at 285.0 eV. Relevantly, the presence of the dominant C-O-C structure had been observed in plasma polymerized epoxy functionalization [22] and epoxy-silane on Si [23], but not in the case of epoxy-silane binding oxidized Si compounds [15, 23].

The progress of the functionalization gave rise to an increasingly complex C1s spectrum, mainly characterized by the a dominant contribution due to the aliphatic carbon, a new C-N contribution at 286.0 eV BE and an additional new N-C=O contribution at 288.3 eV BE, which are characteristic of the presence of immobilized peptides [24]. The C1s spectra from the different stages of biofunctionalization and detection are thus relatively coincident and in line with what obtained in the characterization of protein structures by NAP-XPS at identical conditions [14]. It can be outlined, that detection in NAP-XPS conditions changes the relative contribution of the different species, with a most intense aliphatic carbon contribution at 285.0 eV (figure 3, middle). This is in contrast with what observed in protein [24] and aptamer [25] structures on biosensors characterized by conventional XPS, where C-O polar bonds contribute dominantly to the C1s spectrum, although not generic for any protein structure. This points to an influence of adsorbed water biomolecules on the relative surface exposure of the different residues, which can be controlled by NAP-XPS [14].

We hypothesize that this trend is not general, and that the wetting nature of the surface (hydrophilic vs hydrophobic) may explain the observation of opposite trends according to simulations of protein adsorption [26]. These processes shall be further studied using calibrated aminoacid, peptide and protein monolayers for a clear understanding of the water-biomolecule-surface interaction.

The Au 4f core level spectrum was recorded for the final PSi surface with sandwiched PSA at 100 ng/mL through conjugated AuNPs (figure 3, right). The two observed components are in good agreement with the $4f^{7/2}$ and $4f^{5/2}$ spin orbit splitting of Au and confirmed the successful surface-nanoparticle interaction. Remarkably, the BE of the $4f^{7/2}$ component at 85 eV reflects a +1.0 eV with respect to the referenced BE for metallic Au, This suggests a dominant contribution from the thiol functionalization of the starting AuNPs [27], although the Au surface may be affected by oxidation [28].

Finally, we inspected the structure of the N1s core level for the PSi samples after biofunctionalization with the capture antibody and after sandwich detection (PSA and detection antibody). The spectra shown in figure 4 show that the whole spectrum can be reproduced with three different components, which remained relatively constant as a reflection of the dominant presence of the aminoacid contribution to the overall surface chemistry. A dominant central contribution at 400.0 eV BE is attributed to the peptidic nitrogen, while two small components at higher (402.3 eV) and lower (398 eV) BE reflect the presence of terminal protonated and neutral amine groups, respectively. In spite of the relatively low intensity of the unprotonated component of the N1s peak in protein layers [29], other authors clearly differentiate the splitting between the peptidic nitrogen and the unprotonated amine [30]. In overall, the results are in agreement with a progressive modification of the PSi surface from its electrochemical preparation until its binding with the AuNPs.

3.2 FET detection of PSA

The NiCr contacts deposited on the ion beam carved PSi surface were observed by FE-SEM. A general surface view of the transition from PSi to NiCr demonstrates that the transition is not abrupt with a diffused frontier of 2-3 µm (figure 5.a). The observation at higher magnification on each side of the frontier demonstrated that nanorough surface features decorate both PSi (figure 5.b) and NiCr surfaces (figure 5.c). Since NiCr crystals tend to spread laterally upon nucleation, the diffused surface features are apparently bigger in this case. The cross section views of the PSi substrate show a soft transition to the free surface on uncoated areas (figure 5.d) and columnar structures on the NiCr coated areas (figure 5.e), which may explain the apparently higher surface roughness of the latter areas described above.

The characteristics of the PSi FET structures were measured after completion of the sandwich detection at different concentrations of PSA. Figure 6 (left) shows the variation of the I-V characteristics for different gate voltages for a PSi-FET modified with 5 ng/mL of PSA. It can be observed that at small gate voltages (0,5- 1 V) the current increases steadily with a diode-like behavior. For high gate voltages this behavior does no longer follow (2 V), which suggests a considerable influence of a leakage current in the device. This suggests that comparative measurements for different concentrations of PSA shall be performed at low bias voltages.

Figure 6 (right) shows the I-V response of the PSi-FET structures with different concentrations of PSA at an identical gate voltage of 0.5 V. All the curves follow the above described diode-like exponential increase. Relevantly, the current trend in the PSi-FET characteristics increased in agreement with the increasing amount of PSA, which implies upon performance of the detection step a concomitant increase of AuNPs.

This result confirms previous analysis of PSi-AuNPs systems in which the metal particles contributed to a surface conduction mechanism, which conditions the overall impedimetric response [16]. Only the PSi-FET with 1 ng/mL PSA deviates partially al low surface electrode voltages from the expected response, but the trend is recovered from approximately 0.7 V.

The PSi-FET characteristics at the different PSA concentrations and gate voltage of 0.5 V were used to propose a calibration for the PSi-FET biosensor. The mean conductance $\Delta I/\Delta V$ was estimated from the plots of figure 6 (right) and plotted in a logarithmic scale, as illustrated on figure 7. The results could be fitted to a linear behavior as detailed in the inset of the figure, which also sets the lower limit of detection of PSA with the PSi-FET system in 0.1 ng/mL. These results are relevant from a diagnostics point of view since the clinical range of alarm is estimated at around 5 ng/mL [31].

4. Conclusions

A sandwich biodetection strategy on PSi surfaces has been inspected in a step by step manner in a multi-technique approach. Ellipsometric measurements and photoelectron spectroscopy analyses confirm that the change of surface properties is coherent with a smooth change/transformation of the materials conforming the biointerface from PSi to the bio-organic/AuNPs outer layer. In particular, ellipsometry confirms a progressive deployment of an organic layer from the GPTS silanization, the conjugation with the capture antibody and the final completion of the PSA detection by using AuNPs conjugated with a detection antibody.

The progressive characterization by NAP-XPS provides further insight in the chemical evolution of the biointerface. The steady oxidation of the initially dominant

Si-Si component, the dominant C-O component upon GPTS silanization, and the three component structure of the N1s peak upon conjugation are clear indications of the successful progress of the biofunctionalization cascade. Remarkably, with respect to the use of conventional XPS spectrometers for the characterization of biofunctional PSi, we have found that the initial surface is almost free of adventitious carbon. This suggests that further experiments of transducer surface optimization could be developed and studied in situ with NAP-XPS. Additionally, it is shown that the characteristic C1s peak of the immunologic layer is dominated by the aliphatic carbon component, in contrast with what observed in conventional XPS. This result suggests an influence of the chamber pressure in the conformation of the protein layer, most plausibly due to the role of water in determining the structure of the protein.

The results constitute an evidence of the determinant role that nearly environmental spectroscopic techniques are going to play in the characterization of biomedical interfaces, merging with dynamic techniques to provide complementary structural information.

Acknowledgments

Authors thank L. García Pelayo for his technical assistance during materials processing. We acknowledge MSC funding provided by the European Commission through FP7 grant THINFACE (ITN GA 607232) and from Ministerio de Economía y Competitividad, Spain, through grant SPECTRASENSE (RTC-2017-6311-1).

References

[1] F.A. Harraz, Porous silicon chemical sensors and biosensors: A review, Sensors and Actuators B-Chemical, 202 (2014) 897-912.

[2] K. Hernandez, R. Fernandez-Lafuente, Control of protein immobilization: Coupling immobilization and site-directed mutagenesis to improve biocatalyst or biosensor performance, Enzyme and Microbial Technology, 48 (2011) 107-122.

[3] L.M. Bonanno, L.A. DeLouise, Whole blood optical biosensor, Biosensors & Bioelectronics, 23 (2007) 444-448.

[4] K.S. Chen, S.C. Chen, H.R. Lin, T.R. Yan, C.C. Tseng, A novel technique to immobilize DNA on surface of a quartz crystal microbalance by plasma treatment and graft polymerization, Materials Science & Engineering C-Biomimetic and Supramolecular Systems, 27 (2007) 716-724.

[5] K.S. Kim, H.S. Lee, J.A. Yang, M.H. Jo, S.K. Hahn, The fabrication, characterization and application of aptamer-functionalized Si-nanowire FET biosensors, Nanotechnology, 20 (2009) 235501.

[6] N. Naveas, J. Hernandez-Montelongo, R. Pulido, V. Torres-Costa, R. Villanueva-Guerrero, J.P.G. Ruiz, M. Manso-Silvan, Fabrication and characterization of a chemically oxidized-nanostructured porous silicon based biosensor implementing orienting protein A, Colloids and Surfaces B-Biointerfaces, 115 (2014) 310-316.

[7] M.P. Schwartz, S.D. Alvarez, M.J. Sailor, Porous SiO2 interferometric biosensor for quantitative determination of protein interactions: Binding of protein a to immunoglobulins derived from different species, Analytical Chemistry, 79 (2007) 327-334.

[8] H. Arwin, Ellipsometry on thin organic layers of biological interest: characterization and applications, Thin Solid Films, 377 (2000) 48-56.

[9] M. Bally, M. Halter, J. Voros, H.M. Grandin, Optical microarray biosensing techniques, Surface and Interface Analysis, 38 (2006) 1442-1458.

[10] C. Mao, A.P. Zhu, Q. Wu, X.B. Chen, J.H. Kim, J. Shen, New biocompatible polypyrrole-based films with good blood compatibility and high electrical conductivity, Colloids and Surfaces B-Biointerfaces, 67 (2008) 41-45.

[11] F. Bretagnol, A. Valsesia, G. Ceccone, P. Colpo, D. Gilliland, L. Ceriotti, M. Hasiwa, F. Rossi, Surface functionalization and pPatterning techniques to design

interfaces for biomedical and biosensor applications, Plasma Processes and Polymers, 3 (2006) 443-455.
[12] Y.Y. Liu, Y.L. Ying, X. Hua, Y.T. Long, In-situ discrimination of the water cluster size distribution in aqueous solution by ToF-SIMS, Science China-Chemistry, 61 (2018) 159-163.
[13] G. Olivieri, J.B. Giorgi, R.G. Green, M.A. Brown, 5 years of ambient pressure photoelectron spectroscopy (APPES) at the Swiss Light Source (SLS), Journal of Electron Spectroscopy and Related Phenomena, 216 (2017) 1-16.
[14] M. Kjærvik, K. Schwibbert, P. Dietrich, A. Thissen, W.E.S. Unger, Surface characterisation of Escherichia coli under variousconditions by near-ambient pressure XPS, Surface and Interface Analysis, 50 (2018) 996-1000.
[15] C. Rodriguez, O. Ahumada, V. Cebrian, V.T. Costa, M.M. Silvan, Biofunctional porous silicon micropatterns engineered through visible light activated epoxy capping and selective plasma etching, Vacuum, 150 (2018) 232-238.
[16] C. Rodriguez, V. Torres-Costa, O. Ahumada, V. Cebrian, C. Gomez-Abad, A. Diaz, M.M. Silvan, Gold nanoparticle triggered dual optoplasmonic-impedimetric sensing of prostate-specific antigen on interdigitated porous silicon platforms, Sensors and Actuators B-Chemical, 267 (2018) 559-564.
[17] G. Barillaro, A. Nannini, F. Pieri, L.M. Strambini, Temperature behavior of the APSFET - a porous silicon-based FET gas sensor, Sensors and Actuators B-Chemical, 100 (2004) 185-189.
[18] D. Gallach, V. Torres-Costa, L. Garcia-Pelayo, A. Climent-Font, R.J. Martin-Palma, M. Barreiros-das-Santos, C. Sporer, J. Samitier, M. Manso, Properties of bilayer contacts to porous silicon, Applied Physics a-Materials Science & Processing, 107 (2012) 293-300.
[19] P.M. Kosaka, V. Pini, J.J. Ruz, R.A. da Silva, M.U. Gonzalez, D. Ramos, M. Calleja, J. Tamayo, Detection of cancer biomarkers in serum using a hybrid mechanical and optoplasmonic nanosensor, Nature Nanotechnology, 9 (2014) 1047-1053.
[20] C. Rodriguez, P. Laplace, D. Gallach-Perez, P. Pellacania, R.J. Martin-Palma, V. Torres-Costa, G. Ceccone, M.M. Silvan, Hydrophobic perfluoro-silane functionalization of porous silicon photoluminescent films and particles, Applied Surface Science, 380 (2016) 243-248.

[21] P.M. Dietrich, S. Glamsch, C. Ehlert, A. Lippitz, N. Kulak, W.E.S. Unger, Synchrotron-radiation XPS analysis of ultra-thin silane films: Specifying the organic silicon, Applied Surface Science, 363 (2016) 406-411.

[22] B. Thierry, M. Jasieniak, L. de Smet, K. Vasilev, H.J. Griesser, Reactive epoxy-functionalized thin films by a pulsed plasma polymerization process, Langmuir, 24 (2008) 10187-10195.

[23] C. Funk, P.M. Dietrich, T. Gross, H.G. Min, W.E.S. Unger, W. Weigel, Epoxy-functionalized surfaces for microarray applications: surface chemical analysis and fluorescence labeling of surface species, Surface and Interface Analysis, 44 (2012) 890-894.

[24] L.J. Lai, Y.W. Yang, Y.K. Lin, L.L. Huang, Y.H. Hsieh, Surface characterization of immunosensor conjugated with gold nanoparticles based on cyclic voltammetry and X-ray photoelectron spectroscopy, Colloids and Surfaces B-Biointerfaces, 68 (2009) 130-135.

[25] S. Chung, J.M. Moon, J. Choi, H. Hwang, Y.B. Shim, Magnetic force assisted electrochemical sensor for the detection of thrombin with aptamer-antibody sandwich formation, Biosensors & Bioelectronics, 117 (2018) 480-486.

[26] C.J.D. Foumthuim, A. Corazza, G. Esposito, F. Fogolari, Molecular dynamics simulations of beta-microglobulin interaction with hydrophobic surfaces, Molecular Biosystems, 13 (2017) 2625-2637.

[27] L. Minati, S. Torrengo, G. Speranza, Characterization of gold nanoclusters synthesized on carbon nanotubes film: Evaluation of the size distributions by means of X-ray photoelectron spectroscopy, Surface Science, 604 (2010) 508-512.

[28] C. Vericat, M.E. Vela, G. Benitez, P. Carro, R.C. Salvarezza, Self-assembled monolayers of thiols and dithiols on gold: new challenges for a well-known system, Chemical Society Reviews, 39 (2010) 1805-1834.

[29] S.B. Deng, G. Yu, Y.P. Ting, Production of a bioflocculant by Aspergillus parasiticus and its application in dye removal, Colloids and Surfaces B-Biointerfaces, 44 (2005) 179-186.

[30] I. Tunc, H.H. Susapto, M.O. Guler, Functional gold nanoparticle coated surfaces for CA 125 cancer biomarker detection, Turkish Journal of Chemistry, 39 (2015) 697-713.

[31] D.A. Healy, C.J. Hayes, P. Leonard, L. McKenna, R. O'Kennedy, Biosensor developments: application to prostate-specific antigen detection, Trends in Biotechnology, 25 (2007) 125-131.

Figures

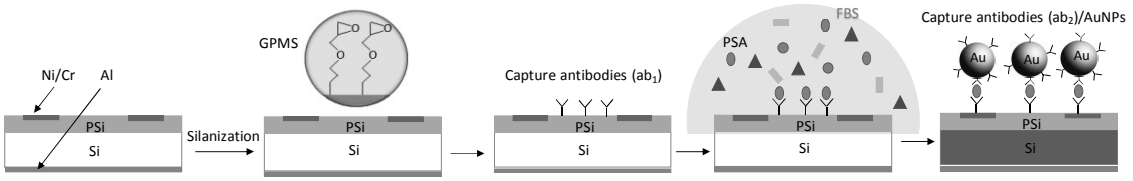

Figure 1. Schematic representation of the preparation of the PSi-AuNPs FET device. The first step corresponds to the FET transducer fabrication, the three intermediate images to the biofunctionalization cascade and the fifth image to the sandwich detection with conjugated AuNPs.

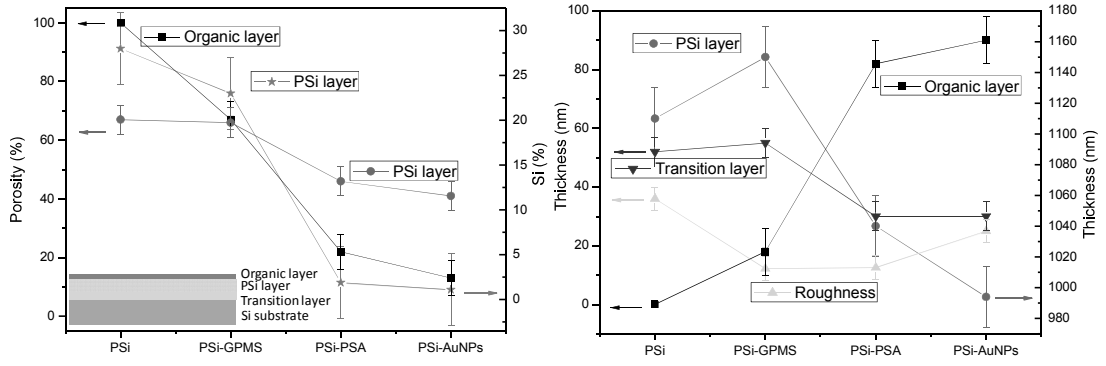

Figure 2. Output parameters from the fitting of the ellipsometric data obtained in the four main steps of preparation of the biosensing device. Left: porosity (air volume fraction in %) for the PSi and Organic layer and inset illustrating the different layers considered for the simulation. Right: fraction of Si remaining in the PSi layer after each biointerface preparation stage. Straight lines just guide the vision. Arrows indicate the relevant axis to each set of scattered data.

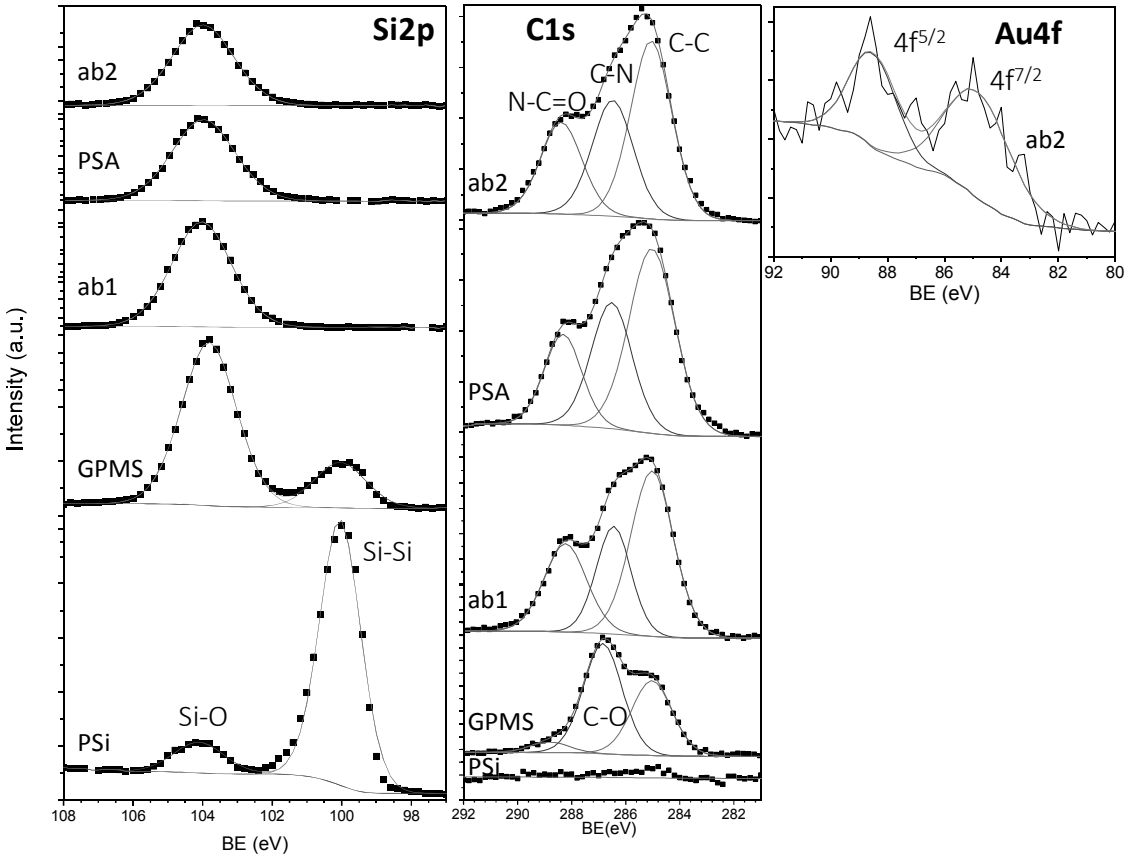

Figure 3. NAP-XPS spectra from the surfaces of PSi at the different stages of biofunctionalization and PSA recognition at 100 ng/mL. (Left) Si2p (Middle) C1s and (Right) Au4f core level spectra (only at 100 ng/mL PSA).

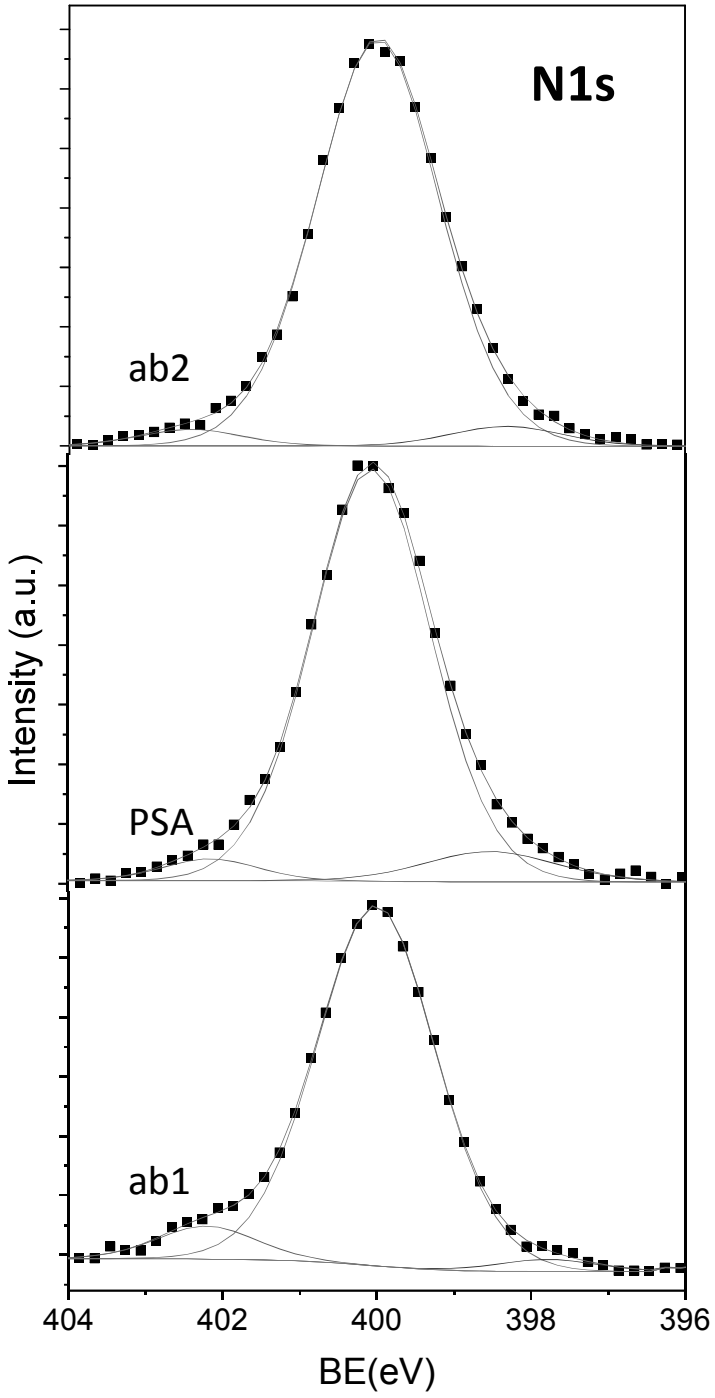

Figure 4. NAP-XPS N1s core level spectra from PSi surfaces after PSA antibody immobilization (top), interaction with PSA (middle) and sandwich assay completion with AuNPs conjugated with the detection antibody at 100 ng/mL (bottom).

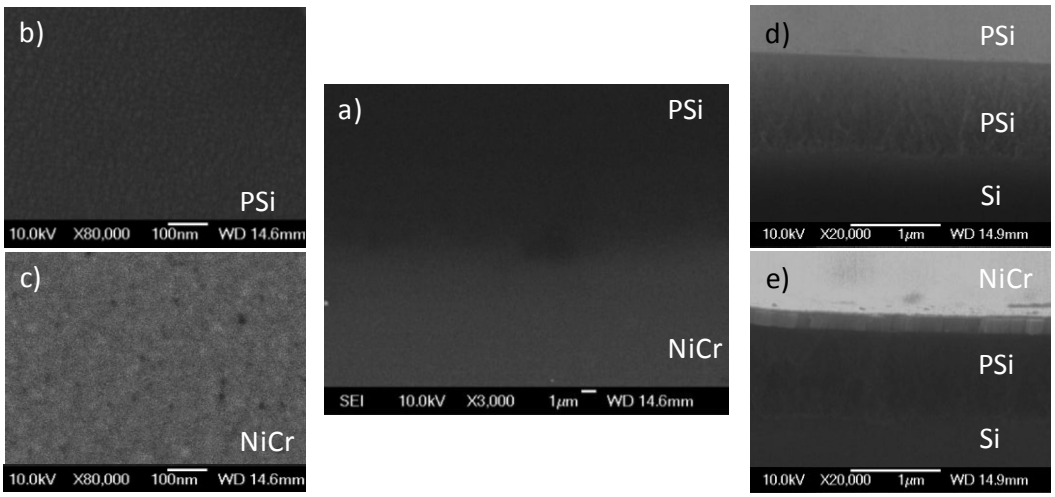

Figure 5. FESEM images of the NiCr contacts performed in carved PSi. Surface view of the transition area from PSi to NiC (a) and higher magnification images of the PSi (b) and NiCr (c) surfaces. Cross section images of the PSi structure in exposed (d) and NiCr coated (e) areas.

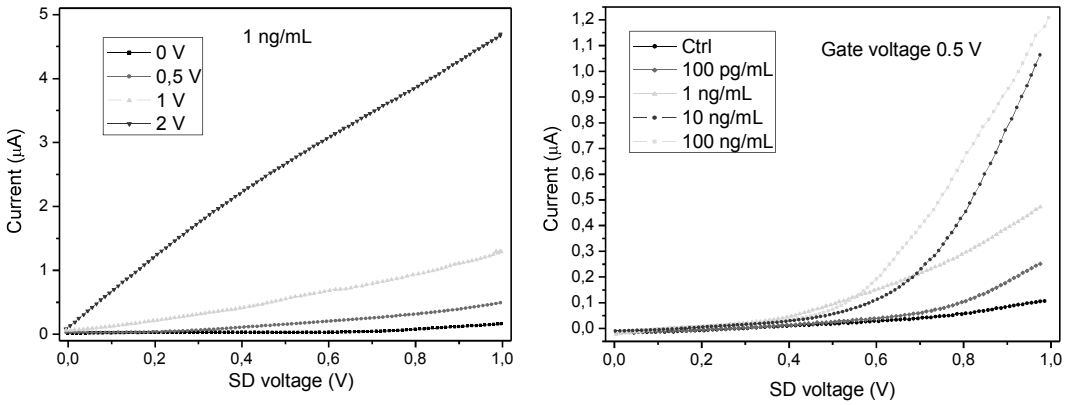

Figure 6. PSi-FET characteristics after recognition with PSA and sandwich with detection antibody conjugated AuNPs. Left, variation of the characteristics for a fixed PSA concentration of 1 ng/mL and different gate voltage. Right, modification of the characteristics for different concentrations of PSA at identical gate voltage of 0.5 V.

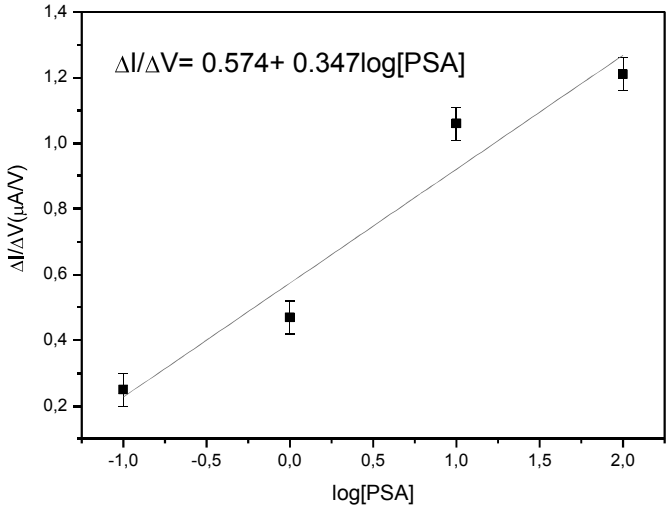

Figure 7. Calibration line for the concentration of PSA as a function of the mean steepness of the characteristic curves of PSi-FET devices measured at 0.5 gate voltage in the 100 to 0.1 ng/mL range.

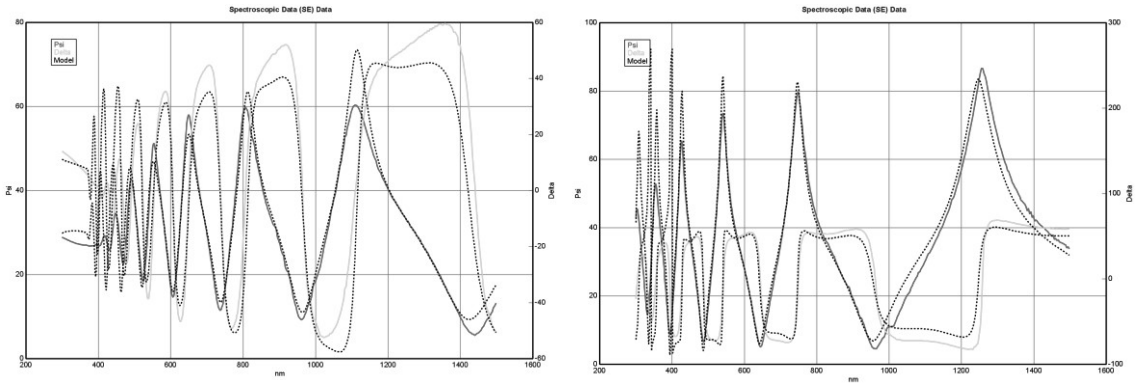

Figure S1. Ellipsometric fitting for the pristine PSi layer (left) and the final PSi+ GPMS+ ab_1+ PSA+ab_2/AuNPs layer after biofunctionalization/recognition cascade (right).